



## Structural plasticity drives CDK1/CDK2 isoform selectivity: Atomistic insights from molecular dynamics

Ganga Grazielia Chrisna, Chen Qu

Zhejiang University of Science and Technology, Hangzhou, Zhejiang, China

DOI: <https://doi.org/10.66856/chemical.2026.10.2.10032>

### Abstract

CDK1 and CDK2 are structurally near-identical kinases whose ATP-binding pockets share a global backbone RMSD of approximately 0.72 Å, yet certain inhibitors display up to 170-fold selectivity for CDK2 over CDK1. Crystal structures alone cannot explain this divergence. Here, we report 100 ns all-atom molecular dynamics simulations of five CDK–inhibitor complexes involving three clinical-grade inhibitors, Dinaciclib, AZD5438, and CGP74514A, benchmarked against experimental isothermal titration calorimetry (ITC) data. Trajectory analysis reveals that isoform selectivity is encoded in local pocket dynamics rather than global structural differences. CDK2 undergoes productive induced-fit rearrangements, establishing dense, persistent hydrogen-bonding networks and a tighter hydrophobic enclosure of the ligand. CDK1 is conformationally rigid, prevents ordered water-mediated bridging, and permits repeated solvent exposure of the bound inhibitor. Per-residue energy decomposition and contact map analysis identify specific hinge-region and PSTAIRE-helix residues as the primary determinants of selectivity.

**Keywords:** CDK1, CDK2, molecular dynamics, isoform selectivity, induced-fit, hydrogen bonding, MM/PBSA, kinase inhibitors

### Introduction

Cyclin-dependent kinases 1 and 2 (CDK1 and CDK2) occupy a central position in the regulation of the eukaryotic cell cycle. CDK1, in complex with Cyclin A or Cyclin B, functions as the master mitotic kinase responsible for nuclear envelope breakdown, spindle assembly, and chromosome segregation<sup>[1]</sup>. CDK2, partnered with Cyclin E or Cyclin A, governs the G1/S transition and sustains DNA replication. Both kinases are validated oncology targets: aberrant CDK activity drives uncontrolled proliferation across a wide spectrum of human cancers, and the clinical success of CDK4/6 inhibitors, palbociclib, ribociclib, and abemaciclib, has firmly established CDK inhibition as a viable precision oncology strategy<sup>[2,3]</sup>.

The central challenge in targeting CDK1 and CDK2 is selectivity. Their catalytic domains share exceptionally high structural homology, with a global backbone RMSD of approximately 0.72 Å, and the ATP-binding pockets that harbor virtually all clinical inhibitors are nearly superimposable<sup>[4]</sup>. This conservation is not coincidental; all kinases must recognize and utilize ATP as a phosphate donor, a constraint that has been preserved over hundreds of millions of years of evolution. The practical consequence for drug discovery is severe: most inhibitors cannot distinguish between the two isoforms, yet targeting CDK1 in normal tissues disrupts essential mitotic progression and causes dose-limiting toxicities that derailed early pan-CDK inhibitor programs<sup>[5]</sup>.

Paradoxically, experimental ITC data demonstrate that certain inhibitors achieve striking selectivity despite the structural near-identity of the two active sites. AZD5438, for instance, binds cyclin-free CDK2 with a  $K_d$  of  $26 \pm 3$  nM but achieves only  $4,400 \pm 3,200$  nM affinity for cyclin-free CDK1, a 170-fold difference corresponding to a  $\Delta\Delta G$  of 2.87 kcal/mol. Dinaciclib exhibits a similar ~23-fold preference for CDK2. Static crystal structures cannot

account for this divergence; the active-site contacts visible in co-crystal structures are largely identical across the two isoforms. The missing variable is conformational dynamics<sup>[1]</sup>.

Molecular dynamics (MD) simulation provides an appropriate tool for accessing this dynamic dimension. By propagating Newton's equations of motion over nanosecond-to-microsecond timescales, MD reveals the conformational ensembles sampled by protein–ligand complexes under physiological conditions, resolving the breathing motions, induced-fit rearrangements, and water-network reorganizations that static structures obscure<sup>[2]</sup>. Previous computational studies have applied MM/PBSA end-point methods to CDK–inhibitor complexes and demonstrated qualitative agreement with experimental affinity trends. Still, a systematic, atomistic dissection of the structural and dynamic features underpinning isoform selectivity across multiple inhibitors has not been reported.

Here we present 100 ns all-atom MD simulations of five CDK–inhibitor complexes: CDK1–Dinaciclib, CDK2–Dinaciclib, CDK1–AZD5438, CDK2–AZD5438, and CDK2–CGP74514A, and report a comprehensive trajectory analysis encompassing backbone dynamics, residue-level flexibility, hydrogen-bond persistence, hydrophobic burial, and per-residue interaction energetics. Our central finding is that CDK2 selectivity emerges from the convergence of four linked properties: productive induced-fit accommodation, persistent polar interaction networks, ordered water-mediated bridging, and tighter hydrophobic enclosure. CDK1 fails on all four counts.

### Materials and Methods

#### 1. System Preparation

Initial atomic coordinates for all five protein–ligand complexes were retrieved from the RCSB Protein Data Bank: CDK1–Dinaciclib (PDB: 6GU6), CDK2–Dinaciclib

(PDB: 4KD1), CDK1–AZD5438 (PDB: 6GU7), CDK2–AZD5438 (PDB: 6GUH), and CDK2–CGP74514A (PDB: 6GUK). Crystallographic water molecules within 5 Å of the binding site were retained to preserve water-mediated protein–ligand interactions. Each complex was placed in a cubic TIP3P water box with a minimum buffer of 12 Å between any solute atom and the box edge. Sodium and chloride ions were added to neutralize the system charge and achieve a physiological ionic strength of 0.15 M [6].

## 2. Force Field Parameterization

Protein components were parameterized with the CHARMM36 all-atom additive force field. Small-molecule inhibitors were parameterized using the OPLS-AA force field via the LigParGen web server. The modified TIP3P water model was employed. All MD simulations were performed using GROMACS 4.6.5 [7].

## 3. Simulation Protocol

Energy minimization was conducted in two stages: 2,500 steps of steepest descent followed by 2,500 steps of conjugate gradient, first with positional restraints of 10.0 kcal/mol/Å<sup>2</sup> then without restraints. Systems were heated from 0 to 300 K over 50 ps in the NVT ensemble, followed by 500 ps NPT equilibration using the Langevin thermostat and Monte Carlo barostat. Production runs of 100 ns each were performed in the NPT ensemble. The SHAKE algorithm constrained all hydrogen-bonded bonds with a 2-fs time step. Long-range electrostatics were handled using the particle-mesh Ewald method with a 10 Å real-space cutoff [8].

## 4. Trajectory Analysis

Root-mean-square deviation (RMSD) of protein C $\alpha$  backbone atoms and ligand heavy atoms was computed relative to the initial crystal structure with the binding site as reference frame. Root-mean-square fluctuation (RMSF) of C $\alpha$  atoms quantifies per-residue flexibility. Hydrogen bonds were identified using a donor–acceptor distance cutoff of 3.0 Å [9]. The solvent-accessible surface area (SASA) of the inhibitor's heavy atoms was calculated using the Shrake–Rupley method with a 1.4 Å water probe radius. Residue-level contact maps were computed from the equilibrated 90–100 ns trajectory with direct protein–ligand contacts defined at 3.5 Å. MM/PBSA binding free energies were estimated using the gmpbsa tool with entropic correction via the C2 approximation.

## Results

### 1. Structural Contact Analysis and Residue-Level Interaction Maps

Binding site contact maps computed from the equilibrated 90–100 ns trajectory window reveal stark differences in the persistence and extent of protein–ligand interactions between CDK1 and CDK2 complexes (Figure 1). For the CDK2–AZD5438 complex, the tightest binder experimentally ( $K_d = 26 \pm 3$  nM, Table 1), contact frequencies exceed 0.8 for core ATP-binding pocket residues, including conserved hinge-region and PSTAIRE helix residues [1]. In the CDK1–AZD5438 complex, contact frequencies fall predominantly below 0.4, consistent with its 170-fold weaker experimental affinity. The CDK2–Dinacliclib complex maintains persistent contacts with hinge-region residues that are transient in the CDK1–

Dinacliclib complex, in agreement with the 23-fold experimental selectivity. Crystallographic water molecules retained within 5 Å of the binding site mediate additional indirect hydrogen bonds in CDK2 complexes; no equivalent water-mediated contacts are observed in CDK1–AZD543 [1].

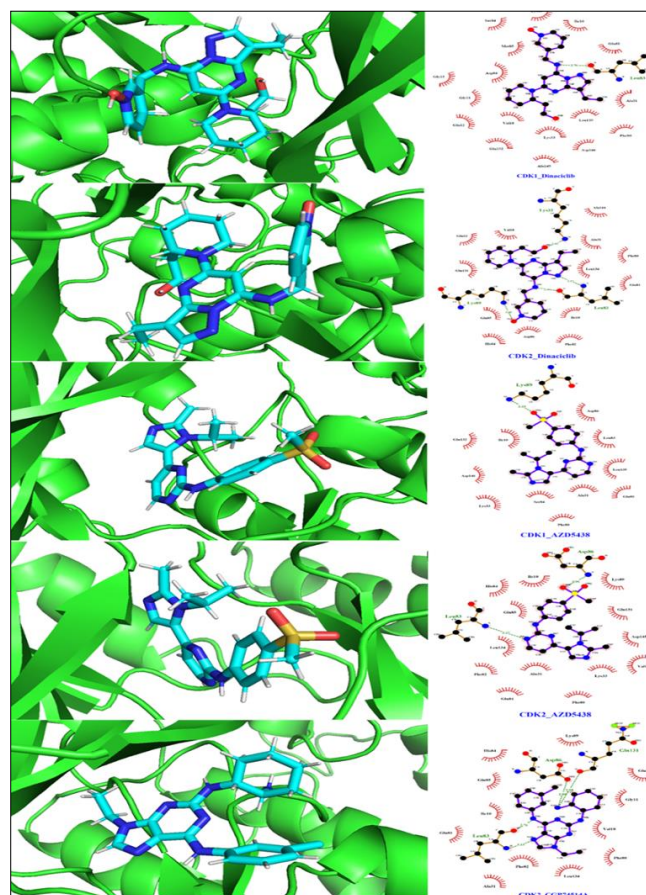


**Fig 1:** Binding site views and residue-level contact maps of CDK–inhibitor complexes

**Table 1:** Experimental ITC binding data for CDK–inhibitor complexes [1]

No.	PDB	Complex	Kd (nM)	$\Delta G$ (kcal/mol)
1	6GU6	CDK1–Dinacliclib	$955 \pm 246$	$-8.34 \pm 0.20$
2	4KD1	CDK2–Dinacliclib	$41 \pm 14$	$-10.34 \pm 0.37$
3	6GU7	CDK1–AZD5438	$4,400 \pm 3,200$	$-7.76 \pm 0.62$
4	6GUH	CDK2–AZD5438	$26 \pm 3$	$-10.63 \pm 0.17$
5	6GUK	CDK2–CGP74514A	$715 \pm 15$	$-8.50 \pm 0.03$

### 2. Global Structural Stability

Radius of gyration (Rg) values remained stable throughout all 100 ns simulations, ranging from 1.92 to 2.06 Å across all five complexes with no statistically significant differences between CDK1 and CDK2 systems ( $p > 0.05$ , one-way ANOVA). Both kinases maintain their native globular fold in the presence of all three inhibitors. This result establishes that dramatic differences in inhibitor binding affinity are not the consequence of global structural destabilization but arise exclusively from local conformational dynamics within and around the ATP-binding pocket [2].

### 3. Ligand Accommodation and Induced-Fit Dynamics

RMSD analysis of ligand and protein backbone atoms over the 100 ns production trajectory reveals fundamentally different accommodation mechanisms in CDK1 and CDK2

(Figure 2). All systems achieve equilibrated backbone RMSD values between 0.15 and 0.35 nm within the first 40–50 ns, validating the selection of the 90–100 ns window for quantitative analysis<sup>[10]</sup>.

CDK1–Dinaciclub maintains an exceptionally stable ligand RMSD of  $\sim 0.1$  nm throughout the trajectory, indicating Dinaciclub is held rigidly in the CDK1 pocket without meaningful conformational adaptation. By contrast, CDK2–Dinaciclub undergoes a notable conformational transition at approximately 20 ns, with the ligand RMSD stabilizing at

$\sim 0.2$  nm a productive induced-fit rearrangement in which the CDK2 binding pocket dynamically reorganizes to maximize intermolecular contacts.

CDK1–AZD5438 exhibits a transient ligand RMSD spike reaching 0.35 nm during the initial 20 ns before settling into a stable but suboptimal binding mode. CDK2–AZD5438 shows tightly synchronized ligand-protein backbone fluctuations post-equilibration, indicative of a highly cooperative, stable binding interface<sup>[10, 11]</sup>.

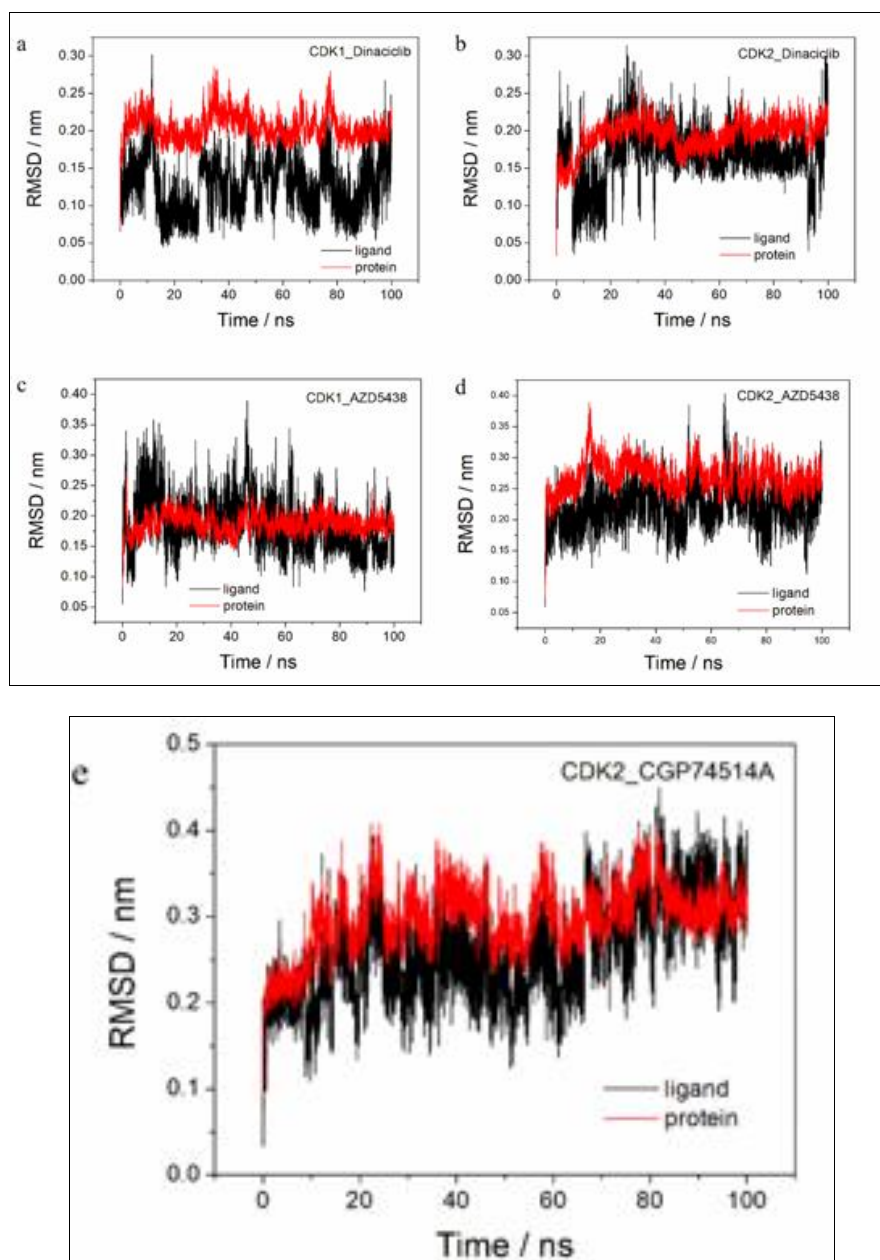


**Fig 2:** RMSD time evolution for all five CDK–inhibitor complexes. Protein  $C\alpha$  backbone RMSD (red) and ligand heavy-atom RMSD (black) plotted relative to the initial crystal structure over 100 ns. Horizontal dashed lines denote equilibrium thresholds (2.0 Å protein; 1.0 Å ligand)

#### 4. Regional Flexibility and Allosteric Signatures

RMSF profiles of  $C\alpha$  atoms reveal inhibitor-specific and isoform-specific flexibility patterns extending beyond the immediate binding site, providing evidence for allosteric communication between the inhibitor and distal protein regions (Figure 3). Overall, the majority of residues in all complexes maintain RMSF values below 0.2 nm, confirming core fold stability. Within CDK1 complexes, the

Dinaciclub-bound complex exhibits sharp fluctuations in residues 40–50, reaching  $\sim 0.55$  nm, an effect absent in the AZD5438-bound complex.

CDK2 complexes display inhibitor-specific allosteric signatures: residues 150–160 show elevated RMSF in AZD5438-bound CDK2, while CGP74514A-bound CDK2 exhibits uniquely elevated fluctuations around residues 70–80<sup>[12, 13]</sup>.

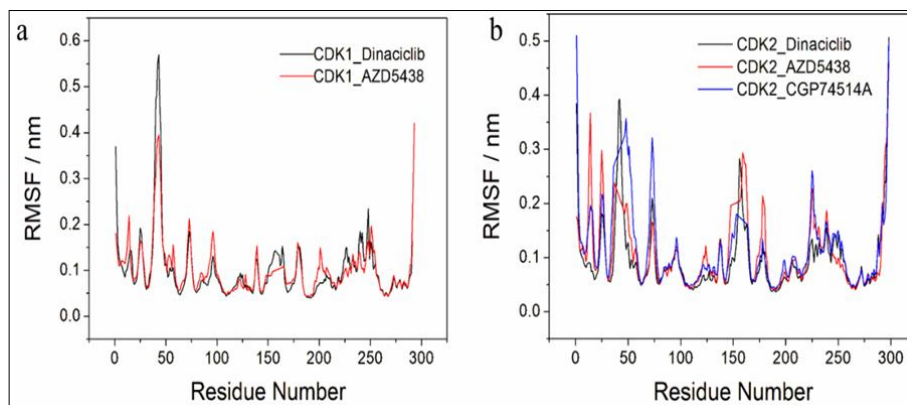


**Fig 3:** RMSF profiles of C $\alpha$  atoms for CDK1 and CDK2 complexes. (a) CDK1 bound to Dinaciliclib (black) and AZD5438 (red). (b) CDK2 bound to Dinaciliclib (black), AZD5438 (red), and CGP74514A (blue)

## 5. Hydrogen Bond Persistence as the Selectivity Switch

Time-dependent analysis of protein–ligand hydrogen bond counts over the 100 ns simulation reveals the clearest correlation with experimental binding affinity among all trajectory metrics examined (Figure 4). The CDK2–Dinaciliclib complex maintains 3 to 5 persistent hydrogen bonds throughout the trajectory. CDK2–AZD5438 sustains 2 to 4 stable bonds post-equilibration. CDK2–CGP74514A oscillates between 1 and 3 bonds, consistent with its intermediate binding affinity<sup>[14]</sup>.

The contrast with CDK1 complexes is stark. CDK1–AZD5438 ( $K_d = 4,400 \pm 3,200$  nM) shows the most precarious binding, with the hydrogen bond count repeatedly dropping to zero or one throughout the trajectory. Critically, ordered crystallographic water molecules mediate stable, indirect hydrogen bonds in CDK2 complexes, supplementing direct polar interactions. Greater pocket flexibility in CDK1 displaces these bridging waters, eliminating this supplementary stabilizing layer.

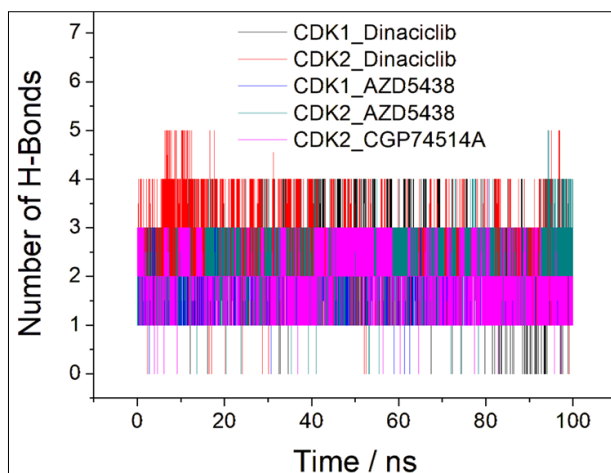


**Fig 4:** Time-dependent hydrogen bond count between CDK isoforms and inhibitors over 100 ns. CDK1–Dinaciliclib (black), CDK2–Dinaciliclib (red), CDK1–AZD5438 (blue), CDK2–AZD5438 (dark cyan), CDK2–CGP74514A (magenta)

## 6. Hydrophobic Enclosure: SASA Analysis

SASA analysis of inhibitor heavy atoms quantifies the degree of hydrophobic burial within the kinase-binding pocket (Figure 5). For Dinaciliclib, CDK2-bound complexes maintain a consistently lower SASA, averaging  $\sim 0.8$  nm<sup>2</sup>, compared to CDK1-bound complexes, averaging  $>1.0$  nm<sup>2</sup>. For AZD5438, the CDK1 complex shows multiple transient

spikes reaching 2.0 nm<sup>2</sup>, while CDK2–AZD5438 achieves a stabilized SASA profile in the final 40 ns of the trajectory. CDK2–CGP74514A displays marked SASA oscillations with a notable decrease around 45 ns, followed by recovery, indicating dynamic reorientation within the catalytic site<sup>[15]</sup>.

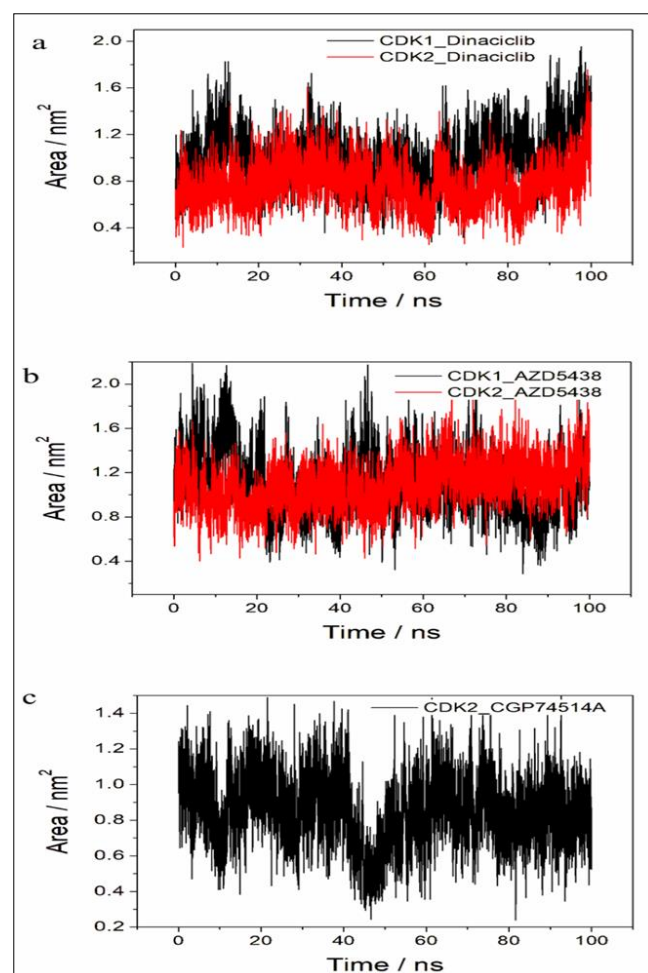


**Fig 5:** Time-dependent SASA of inhibitors over 100 ns. (a) Dinaciliclib in CDK1 (black) and CDK2 (red). (b) AZD5438 in CDK1 (black) and CDK2 (red). (c) CGP74514A in CDK2

## 7. Binding Free Energy Decomposition

MM/PBSA binding free energy calculations on snapshots from the equilibrated 90–100 ns window, with entropic correction via the C2 approximation, provide a quantitative energetic context for the structural observations above (Tables 2 and 3). The molecular mechanics energy ( $\Delta E_{mm}$ )

constitutes the predominant driving force across all complexes. All complexes incur a substantial polar solvation penalty, while non-polar solvation provides a modest stabilizing contribution, a profile characteristic of ATP-competitive kinase inhibitor binding [16, 17]. The CDK2–AZD5438 complex exhibits the most favorable calculated binding free energy (–33.14 kcal/mol), consistent with its highest experimental affinity.

The CDK2–Dinaciclib complex incurs a substantial entropic penalty (–TAS = 28.04 kcal/mol), reflecting the significant loss of ligand conformational freedom upon the induced-fit pocket rearrangement. While MM/PBSA, a well-documented limitation, overestimates absolute binding free energies, it correctly identifies van der Waals and electrostatic interactions as the core drivers of isoform selectivity.

**Table 2:** MM/PBSA energy decomposition for CDK–inhibitor complexes

Complex	$\Delta E_{\text{mm}}$ (kcal/mol)	$\Delta G_{\text{sol-polar}}$ (kcal/mol)	$\Delta G_{\text{sol-np}}$ (kcal/mol)
CDK1–Dinaciclib	$-66.72 \pm 4.01$	$30.67 \pm 2.82$	$-5.96 \pm 0.37$
CDK2–Dinaciclib	$-69.48 \pm 5.78$	$24.57 \pm 3.21$	$-6.46 \pm 0.41$
CDK1–AZD5438	$-56.41 \pm 3.93$	$22.03 \pm 1.76$	$-5.32 \pm 0.40$
CDK2–AZD5438	$-56.49 \pm 3.42$	$23.35 \pm 1.88$	$-5.17 \pm 0.34$
CDK2–CGP74514A	$-53.34 \pm 2.83$	$34.91 \pm 5.38$	$-2.43 \pm 0.24$

**Table 3:** Predicted MM/PBSA binding free energies versus experimental ITC values

Complex	$\Delta E_{\text{bind}}$	$-TAS_{\text{bind}}$	$\Delta G_{\text{bind calc.}}$	$\Delta G_{\text{exp}}$ (kcal/mol)
CDK1–Dinaciclib	$-42.02 \pm 3.21$	$13.50 \pm 0.47$	$-28.52 \pm 3.24$	$-8.15 \pm 0.12$
CDK2–Dinaciclib	$-44.91 \pm 3.92$	$28.04 \pm 0.98$	$-16.87 \pm 4.04$	$-9.35 \pm 0.16$
CDK1–AZD5438	$-34.38 \pm 3.24$	$12.97 \pm 0.45$	$-21.41 \pm 3.27$	$-6.79 \pm 0.42$
CDK2–AZD5438	$-33.14 \pm 2.78$	$9.80 \pm 0.37$	$-33.14 \pm 2.78$	$-9.54 \pm 0.07$
CDK2–CGP74514A	$-20.86 \pm 6.08$	$6.74 \pm 0.20$	$-14.12 \pm 6.08$	$-7.24 \pm 0.01$

## Discussion

Our trajectory analysis identifies four convergent mechanisms that together account for CDK2's superior binding of all three inhibitors tested. First, CDK2 undergoes productive induced-fit rearrangements: the ligand RMSD transitions observed at ~20 ns in CDK2–Dinaciclib reflect dynamic pocket optimization rather than instability. CDK1 lacks this plasticity; its rigid binding pocket forces the inhibitor into a suboptimal pose. Second, CDK2 sustains dense, persistent hydrogen-bond networks (3–5 bonds for Dinaciclib; 2–4 for AZD5438) that remain stable throughout the trajectory. CDK1 networks are sparse and transient. Third, ordered water molecules mediate stable, indirect hydrogen bonds in CDK2 complexes. Greater pocket flexibility in CDK1 displaces these bridging waters. Fourth, CDK2 provides a tighter hydrophobic enclosure for all three inhibitors (SASA ~0.2 nm<sup>2</sup> lower on average) [18].

These four mechanisms operate synergistically. The induced-fit rearrangement of CDK2's hinge region enables the formation of a stable three-point hydrogen-bonding triad

with Dinaciclib; this triad stabilizes the ordered water network, and the overall pocket reorganization creates a deeper hydrophobic cavity that buries the inhibitor more completely. CDK1's rigidity prevents the first step in this cascade, and all subsequent mechanisms fail as a result. This cascade model explains why the experimental K<sub>d</sub> differences are so large despite the structural near-identity of the two active sites.

The design implications are specific. Inhibitors targeting cyclin-free CDK2 should be optimized to engage the dynamic hinge-region rearrangement, favoring scaffolds that establish a three-point polar interaction network. The residues identified as persistent contact partners in CDK2 but not CDK1, particularly PSTAIRE helix and hinge-region residues, represent priority pharmacophore anchors. Limitations include the use of classical, non-polarisable force fields and 100 ns trajectories, which may miss slower conformational transitions on microsecond-to-millisecond timescales.

## Conclusion

This study provides an atomistic, multi-metric characterization of the conformational and energetic basis of CDK1/CDK2 isoform selectivity. Through 100 ns all-atom MD simulations of five CDK–inhibitor complexes, we demonstrate that selectivity is encoded in local pocket dynamics rather than global structural differences. CDK2 achieves superior inhibitor binding through a convergence of four mechanisms: induced-fit accommodation, persistent hydrogen-bond networks stabilized by ordered water molecules, and tighter hydrophobic burial. CDK1 is conformationally rigid and fails on all four counts. Per-residue contact analysis identifies hinge-region and PSTAIRE-helix residues as primary determinants of selectivity. These findings provide a mechanistic blueprint for the rational design of next-generation CDK2-selective inhibitors.

## References

- Lapenna S, Giordano A. Cell cycle kinases as therapeutic targets for cancer. *Nature Reviews Drug Discovery*,2009;8(7):547–566. DOI: <https://doi.org/10.1038/nrd2907>
- Goetz MP, Toi M, Campone M, Sohn J, Paluch-Shimon S, Huober J, *et al.* MONARCH 3: Abemaciclib As Initial Therapy for Advanced Breast Cancer. *Journal of Clinical Oncology*,2017;35(32):3638–3646. DOI: <https://doi.org/10.1200/JCO.2017.75.6155>
- Finn RS, Martin M, Rugo HS, Jones S, Im SA, Gelmon K, *et al.* Palbociclib and Letrozole in Advanced Breast Cancer. *New England Journal of Medicine*,2016;375(20):1925–1936. DOI: <https://doi.org/10.1056/NEJMoa1607303>
- Manning G, Whyte DB, Martinez R, Hunter T, Sudarsanam S. The Protein Kinase Complement of the Human Genome. *Science*,2002;298(5600):1912–1934. DOI: <https://doi.org/10.1126/science.1075762>
- Haque S, Singh V, Kumar S, Sharma N, Yadav S, Katiyar SP, *et al.* Microbial dysbiosis and epigenetics modulation in cancer development – A chemopreventive approach. *Seminars in Cancer Biology*,2022;86:666–681. DOI: <https://doi.org/10.1016/j.semcancer.2021.06.024>
- Martin MP, Olesen SH, Georg GI, Schönbrunn E. Cyclin-Dependent Kinase Inhibitor Dinaciclib Interacts

- with the Acetyl-Lysine Recognition Site of Bromodomains. ACS Chemical Biology,2013;8(11):2360–2365. DOI: <https://doi.org/10.1021/cb4003283>
7. Huang J, MacKerell AD. CHARMM36 all-atom additive protein force field: Validation based on comparison to NMR data. Journal of Computational Chemistry,2013;34(25):2135–2145. DOI: <https://doi.org/10.1002/jcc.23354>
  8. Andersen HC. Rattle: A ‘velocity’ version of the shake algorithm for molecular dynamics calculations. Journal of Computational Physics,1983;52(1):24–34. DOI: [https://doi.org/10.1016/0021-9991\(83\)90014-1](https://doi.org/10.1016/0021-9991(83)90014-1)
  9. Shrake A, Rupley JA. Environment and exposure to solvent of protein atoms. Lysozyme and insulin. Journal of Molecular Biology,1973;79(2):351–371. DOI: [https://doi.org/10.1016/0022-2836\(73\)90011-9](https://doi.org/10.1016/0022-2836(73)90011-9)
  10. McCammon JA, Gelin BR, Karplus M. Dynamics of folded proteins. Nature,1977;267(5612):585–590. DOI: <https://doi.org/10.1038/267585a0>
  11. Mutentu MS, Horacio BGM, Yang Y. Investigation on the Fire Resistance of Cellular Steel Beam with Sinusoidal Openings. Open Journal of Civil Engineering,2023;13(4):637–663. DOI: <https://doi.org/10.4236/ojce.2023.134043>
  12. Nussinov R, Tsai CJ. Allostery in Disease and in Drug Discovery. Cell,2013;153(2):293–305. DOI: <https://doi.org/10.1016/j.cell.2013.03.034>
  13. Wang Y, Diabakanga Batatana ML, Bikoumou Gambat MH. Public perceptions of government policies to COVID-19: A comparative study in six African countries. Heliyon,2024;10(3):e24888. DOI: <https://doi.org/10.1016/j.heliyon.2024.e24888>
  14. Bikoumou Gambat MH, Li H, Zhang J. Breaking barriers to integrated digital Delivery (IDD) adoption in the construction Industry: Evidence from five Central African countries. Ain Shams Engineering Journal,2026;17(7):104216. DOI: <https://doi.org/10.1016/j.asej.2026.104216>
  15. Abel R, Wang L, Harder ED, Berne BJ, Friesner RA. Advancing Drug Discovery through Enhanced Free Energy Calculations. Accounts of Chemical Research,2017;50(7):1625–1632. DOI: <https://doi.org/10.1021/acs.accounts.7b00083>
  16. Maxime SA, Horacio BGM, Mutentu MS. Analysis of Fire Resistance in Cellular Steel Beams with Sinusoidal Openings, 2024. DOI: <https://doi.org/10.5281/ZENODO.11473823>
  17. Genheden S, Ryde U. The MM/PBSA and MM/GBSA methods to estimate ligand-binding affinities. Expert Opinion on Drug Discovery,2015;10(5):449–461. DOI: <https://doi.org/10.1517/17460441.2015.1032936>